Proc. Natl. Acad. Sci. USA
Vol. 90, pp. 9542–9546, October 1993
Biochemistry

Peptide nucleic acid (PNA) conformation and polymorphism in PNA–DNA and PNA–RNA hybrids

(chimera/duplex/triple helix/molecular mechanics)

ÖRN ALMARSSON AND THOMAS C. BRUICE

Department of Chemistry, University of California at Santa Barbara, Santa Barbara, CA 93106

Contributed by Thomas C. Bruice, July 19, 1993

ABSTRACT **Two hydrogen-bonding motifs have been proposed to account for the extraordinary stability of polyamide "peptide" nucleic acid (PNA) hybrids with nucleic acids. These interresidue- and intraresidue-hydrogen-bond motifs were investigated by molecular mechanics calculations. Energy-minimized structures of Watson–Crick base-paired decameric duplexes of PNA with A-, B-, and Z-DNA and A-RNA polymorphs indicate that the inherent stability of the complementary PNA helical structures is derived from interresidue, rather than from intraresidue, hydrogen bonds in all hybrids studied. Intraresidue-hydrogen-bond lengths are consistently longer than interresidue hydrogen bonds. Helical strand stability with interresidue hydrogen bond stabilization follows the order: B-(DNA·PNA) > A-(DNA·PNA) ≈ A-RNA·PNA > Z-(DNA·PNA). In the triplex hybrids A-(RNA·PNA_2) and B-(DNA·PNA_2), differences between stabilities of the two decamers of thyminyl PNA with lysine amide attached to the C terminus $({}_{pna}T)_{10}$ strands are small. The Hoogsteen $({}_{pna}T)_{10}$ strands are of slightly higher potential energy than are the Watson–Crick $({}_{pna}T)_{10}$ strands. Antiparallel arrangement of PNAs in the triplex is slightly favored over the parallel arrangement based on the calculations. Examination by molecular mechanics of the PNA·DNA analogue of the NMR-derived structure for the B-double-stranded DNA dodecamer d(CGCAAATTTGCG)$_2$ in solution suggests that use of all bases of the genetic alphabet should be possible without loss of the specific interresidue-hydrogen-bonding pattern within the PNA strand.**

Nucleic acid recognition by antisense agents has been an area of intense scientific effort for quite some time (1). An approach that has attracted considerable attention in the development of polymeric structures that can replace single-stranded DNA or RNA is the use of peptide-nucleic acid surrogates (2). A recent advance in this field is the design and synthesis of the polyamide "peptide" nucleic acid (PNA) chimera (Scheme I).

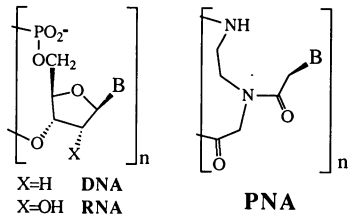

Scheme I

Polymeric PNA structures are composed of 2-aminoethyl glycine units with the glycyl nitrogen acylated by an acetate linker to a nucleobase (3, 4). A proposed advantage of PNAs as antisense agents, compared with phosphate diester-linked nucleic acids, is their stability toward nucleases. Although the designing of the PNA analogues of DNA has been described by the inventors (4), the design rationale does not explain the great stability of the PNA hybrids with nucleic acids, as exemplified by PNA-strand invasion of double-helical DNA. Our recent molecular mechanics study (5) with the B-helix structure of the DNA·PNA duplex $(dAp)_{10}$·$({}_{pna}T)_{10}$ [where $(dAp)_{10}$ is the decanucleotide of 2′-deoxyadenosine 5′-phosphate and $({}_{pna}T)_{10}$ is the decamer of thyminyl PNA with lysine amide attached to the C terminus] strongly suggests that the stability of DNA·PNA duplexes is due to interresidue hydrogen bonding between PNA polyamide units as shown in Scheme II and Fig. 1.

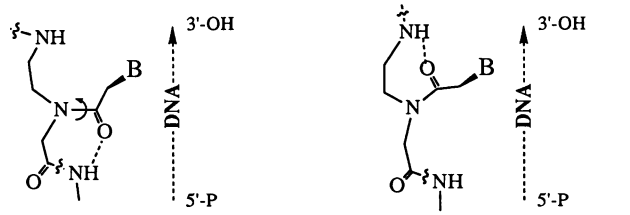

Scheme II

To further understand the importance of internal hydrogen bonding in helical PNA·DNA structures we now examine intraresidue and interresidue hydrogen bonding as a means of PNA-strand stabilization in the conformations required for complementarity with A-, B-, and Z-helical strands of DNA (and A-RNA). The question whether the most stable structures are obtained when the two PNA strands are parallel or antiparallel in the triplex structures B-{$(dAp)_{10}$·[$({}_{pna}T)_{10}$]$_2$} and A-{$(Ap)_{10}$·[$({}_{pna}T)_{10}$]$_2$} [where $(Ap)_{10}$ is the decanucleotide of adenosine 5′-phosphate] was also addressed. Molecular mechanics calculations of the structure of a DNA·PNA analogue based on the solution NMR structure (6) for the B-DNA dodecamer d(CGCAAATTTGCG)$_2$ was performed to assess the viability of interresidue hydrogen bonds in a generic sequence of DNA incorporating all bases.

MATERIALS AND METHODS

All computational analyses and graphical visualization were done on a Silicon Graphics model 4D/320GTX workstation. Quanta version 3.3 (1993) Nucleic Acid Builder (Molecular Simulations, Waltham, MA) was used to generate the two complementary decamers of single-stranded DNA in an A-conformation, as prescribed in the DNAH.RTF topology file for CHARMM version 2.2 (1993) (Molecular Simulations, ref.

The publication costs of this article were defrayed in part by page charge payment. This article must therefore be hereby marked "*advertisement*" in accordance with 18 U.S.C. §1734 solely to indicate this fact.

Abbreviations: PNA, polyamide "peptide" nucleic acid; $(dAp)_{10}$, decanucleotide of 2′-deoxyadenosine 5′-phosphate; $(Ap)_{10}$, decanucleotide of adenosine 5′-phosphate; $({}_{pna}T)_{10}$, decamer of thyminyl PNA with lysine amide attached to the C terminus; ds, double stranded.

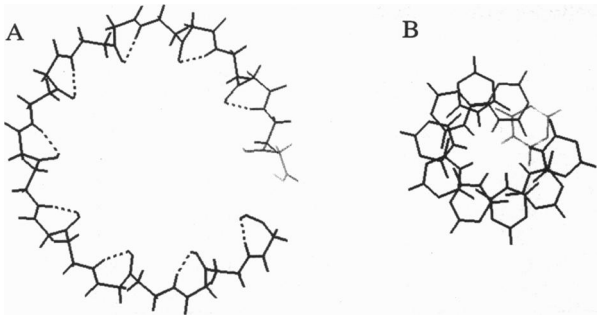

FIG. 1. Views along the helical axis of PNA ($_{pna}T)_{10}$ strand in a conformation complementary to B-DNA sequence $(dAp)_{10}$. (*A*) Proposed interresidue hydrogen bonds in backbones of PNA sequences (dashed lines). (*B*) Stick model of nucleic acid bases in the helical ($_{pna}T)_{10}$ strand, showing alignment of thymines around the helical axis.

7). Hybrid molecules with PNAs with interresidue hydrogen bonds were constructed as described (5). Structures where intraresidue hydrogen bonds operate were built by overlaying the DNA strand with the PNA structure as follows: The linker $-CH_2C(=O)-$ units were overlaid on the positions formerly occupied by the C1′ carbon and oxygen of the ribose ring. The PNA glycine nitrogen, α-carbon, and C(=O) were superimposed on C4′, C3′, and O3′, respectively, whereas the $-CH_2CH_2NH-$ units were superimposed on C5′, O5′, and the phosphorous, respectively. All hydrogens were included on both PNA and nucleic acid strands. A CHARMM topology file (RTF) was written for all units of PNA by consideration of charges and atom types in DNA (as in DNAH.RTF) and glycine (as in AMINOH.RTF) (5). A sodium ion with a charge of +1.0 was added to each nucleotide residue in DNAH.RTF and RNAH.RTF. The neutral duplex decamers of complementary PNAs and DNA $[(dAp)_{10}\cdot(_{pna}T)_{10}]$ and RNA $[(Ap)_{10}\cdot(_{pna}T)_{10}]$ were minimized in CHARMM as described (5). Suitable distance constraints for the Watson–Crick base pairs (8) were applied throughout minimizations. Hydrogen bonds and nonbonding interactions were cut off at 5.0 and 14.0 Å, respectively, and angle cut-off for hydrogen bonding was set at 90°. Total energies were calculated for the PNA strand in the required conformation for each helix type. The x-ray coordinates for the Z-DNA dodecamer $d\{[(_{anti}Cp)(_{syn}Gp)]_6\}_2$ (Protein Data Bank file pdb3zna.ent) (9) were used as a basis for a duplex hybrid with a complementary PNA strand. The $d[(_{anti}Cp)(_{syn}Gp)]_6\cdot[_{pna}(GC)]_6$ hybrid was constructed by a method analogous to that used to build decameric hybrids. A solution structure for a dodecameric B-DNA with the sequence $d(CGCAAATTTGCG)_2$ (6) was similarly used to create the d(CGCAAATTTGCG)/($_{pna}$CGCTTTAAACGC) hybrid.

The model building of the triple helix with PNA strands antiparallel and complementary to a B-DNA conformation follows from our previous modeling of triple helical B-DNA·PNA_2 D-loop structure (5). The Hoogsteen base-paired third strand in the B-(PNA_2·DNA) complex, where the PNA strands are parallel, was created by (*i*) cutting the backbone away from the thymines in the Hoogsteen strand of the starting structure with the PNAs antiparallel, (*ii*) rotating the backbone to bring it into a parallel arrangement with the PNA in the Watson–Crick paired strand, and (*iii*) reconnecting the backbone to the bases. Steepest-descent minimizations with atom constraints on positions of all bases, as well as the DNA segment and Watson–Crick PNA strand, were then applied with distance constraints to fit the backbone properly to the bases again. Suitable distance constraints were placed on both Watson–Crick and Hoogsteen base pairs of the parallel strand with the purines of the DNA strand (8) during subsequent energy minimization. Similar procedures yielded the A-$\{(Ap)_{10}\cdot[(_{pna}T)_{10}]_2\}$ hybrid triplex with parallel T_{10} strands. A-$\{(Ap)_{10}\cdot[(_{pna}T)_{10}]_2\}$ with antiparallel PNA strands was constructed from A-$[(Ap)_{10}\cdot(_{pna}T)_{10}]$, and the Hoogsteen-paired ($_{pna}T)_{10}$ was constructed from B-$\{(dAp)_{10}\cdot[(_{pna}T)_{10}]_2\}$ with antiparallel PNAs. The connections between the backbone and bases in the Hoogsteen strand were severed, the alignment of the thymines in the major groove was manually fixed to accord with the ideal Hoogsteen base-pair arrangement (8), and finally the backbone was reconnected.

RESULTS AND DISCUSSION

In a previous study of the double-stranded (ds) DNA·PNA duplex B-$[(dAp)_{10}\cdot(_{pna}T)_{10}]$ we provided evidence that interresidue hydrogen bonding stabilizes the helical PNA strands (5). Modeling of A-(RNA·PNA) and A-(DNA·PNA) hybrids has not been investigated. Despite the larger helical rise per base pair in the A-conformation (≈3.4 Å compared with 2.6 Å in B-DNA) and a longer distance between phosphorous atoms in adjacent nucleotides (7.0 Å compared with 5.9 Å in B-DNA), modeling of the ($_{pna}T)_{10}$ sequence onto the pyrimidine strand of A-RNA to provide A-$[(Ap)_{10}\cdot(_{pna}T)_{10}]$ is easily accomplished (Fig. 2). By inspection of the stereoview of the energy-minimized structure in Fig. 2 one can observe the interresidue hydrogen bonds (*a* in Scheme II). Table 1 lists molecular mechanics potential energies for the ($_{pna}T)_{10}$ strand separated from the $[(Ap)_{10}\cdot(_{pna}T)_{10}]$, when fixed in the conformation required by the A-type helix. The structure for A-dsDNA was used to model the structure of A-$[(dAp)_{10}\cdot(_{pna}T)_{10}]$, and the pertinent potential energies are included in Table 1. The energy-minimized structure for A-(DNA·PNA) is quite similar to the structure in Fig. 2 for the A-(RNA·PNA) hybrid. The potential energies of the ($_{pna}T)_{10}$ strands in A-$[(Ap)_{10}\cdot(_{pna}T)_{10}]$ and A-$[(dAp)_{10}\cdot(_{pna}T)_{10}]$ are nearly identical (see top half of Table 1), although their conformations

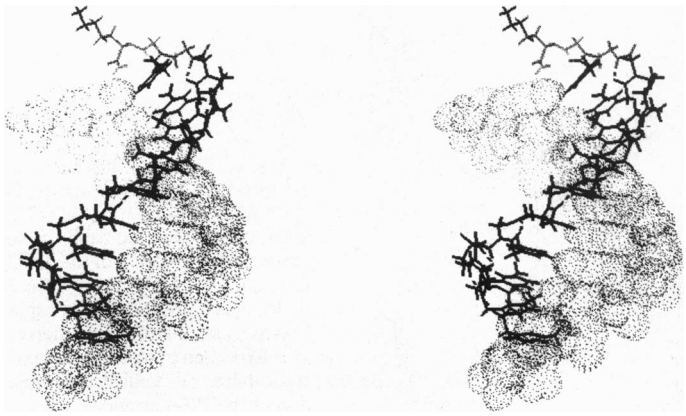

FIG. 2. Stereoview of structure of $(Ap)_{10}\cdot(_{pna}T)_{10}$ RNA·PNA hybrid duplex. The RNA strand, displayed as a van der Waals dot surface, is in an A-conformation. The helical conformation of the PNA is stabilized by interresidue hydrogen bonds shown as dashed lines (see *a* in Scheme II).

Table 1. Total CHARMM energies and individual energy contributions for separated single-stranded $(_{pna}T)_{10}$ constituents of decameric $(dAp)_{10}\cdot(_{pna}T)_{10}$ possessing *inter*residue and *intra*residue hydrogen bonds

$(_{pna}T)_{10}$ structure	Form	Energy*	Bond	Angle	Dihedral	Impr	VDW	Elec	H bond
Interresidue H bond†	A-RNA	−1367	14.3	101	47.1	3.0	−80.0	−1435	−17.6
	A-DNA	−1385	13.8	100.1	45.2	4.5	−78.6	−1449	−21.6
	B-DNA	−1473	15.6	88.4	47.5	4.0	−72.5	−1531	−25.4
	Z-DNA	−1363	11.6	86.7	52.4	7.7	−52.9	−1447	−21.2
Intraresidue H bond‡	A-RNA	−1179	15.2	97.3	45.1	4.4	−84.4	−1239	−17.1
	A-DNA	−1173	14.6	93.5	59.3	4.7	−78.8	−1250	−16.6
	B-DNA	−1348	14.7	82.7	52.4	6.2	−80.5	−1404	−18.9
	Z-DNA	−1388	12.8	91.3	48.8	7.2	−57.1	−1465	−25.3

See ref. 8 for details of the CHARMM force-field contributions; see text for PNA structure.
*CHARMM total energy in kcal/mol, sum of all individual contributions. Impr, improper dihedral; VDW, van der Waals; Elec, electronic.
†*a* in Scheme II.
‡*b* in Scheme II.

differ slightly [rms deviations between these $(_{pna}T)_{10}$ structures with hydrogens included is 0.38 Å].

Recent reports indicate that formation of a ds(DNA·PNA) duplex is not limited to $ds[(_{pna}T)_n\cdot(dAp)_n]$. Sequences of PNA form 1:1 complexes with their complementary DNA sequence, regardless of the identity of the nucleobases (10–12). To assess whether base sequence affects the contiguous intrastrand hydrogen bonds in PNA, the structure for a PNA·DNA hybrid of the B-DNA dodecamer d(CGCAAATTTGCG)$_2$ was constructed by replacement of a DNA strand with corresponding PNA sequence. The initial coordinates for the bases and complementary DNA strand was obtained from an NMR solution structure (6) for this B-DNA in water. Fig. 3 displays a stereo model of the structure of d(CGCAAATTTGCG)/($_{pna}$CGCAAATTTGCG), where the latter strand is a PNA polymer. The interresidue hydrogen bonds are retained in the PNA strand, despite the base sequence variation.

In the left-handed Z-form of DNA, which is confined to sequences of repeating units of alternating purines and pyrimidines (usually guanine and cytosine), the purine is in the syn conformation relative to the deoxyribose ring, whereas the pyrimidine is in the anti-conformation (13). The result is a zig-zag linking of the nucleotides in the Z-DNA. This combination presents an interesting challenge for PNA recognition. A structure for the duplex Z-DNA dodecamer of $d\{[(_{anti}Cp)(_{syn}Gp)]_6\}_2$ (9) was transformed to give the corresponding hybrid duplex with PNA. The energy-minimized duplex structure of $d\{[(_{anti}Cp)(_{syn}Gp)]_6\}\cdot[_{pna}(CG)_6]$ is shown in stereoview in Fig. 4. Without the steric constraints of the deoxyribose ring, the $(_{pna}CG)_6$ strand can be brought into a conformation that allows contiguous interresidue hydrogen bonds. For comparison purposes with the molecular mechanics-calculated A- and B-helical hybrids, the hypothetical structure of Z-$[(dAp)_{10}\cdot(_{pna}T)_{10}]$ was constructed. The calculated potential energy for the PNA component of Z-$[(dAp)_{10}\cdot(_{pna}T)_{10}]$, along with energies for PNA strands of other duplexes, is included in Table 1.

With interresidue hydrogen bonds included, the energies for $(_{pna}T)_{10}$ strands of A-$[(Ap)_{10}\cdot(_{pna}T)_{10}]$, A-$[(dAp)_{10}\cdot(_{pna}T)_{10}]$, Z-$[(dAp)_{10}\cdot(_{pna}T)_{10}]$, and B-$[(dAp)_{10}\cdot(_{pna}T)_{10}]$ with interresidue hydrogen bonds are included in the top half of Table 1. The calculated order of stabilities of $(_{pna}T)_{10}$ strands is B-$[(dAp)_{10}\cdot(_{pna}T)_{10}]$ > A-$[(dAp)_{10}\cdot(_{pna}T)_{10}]$ ≃ A-$[(Ap)_{10}\cdot(_{pna}T)_{10}]$ > Z-$[(dAp)_{10}\cdot(_{pna}T)_{10}]$. Examination of the various force-field contributions (Table 1) shows that single-stranded DNA in the conformations found in A- and B-DNA as well as single-stranded RNA in ds(A-RNA) all appear to provide good complementarity with interresidue-hydrogen-bonded PNA strands. Inspection of the top half of Table 1 reveals that electronic, hydrogen-bonding, and angle-deformation energies favor the B-(DNA·PNA) hybrid.

The relative importance of intraresidue vs. interresidue hydrogen bonding (Scheme II) as stabilizing influences in the

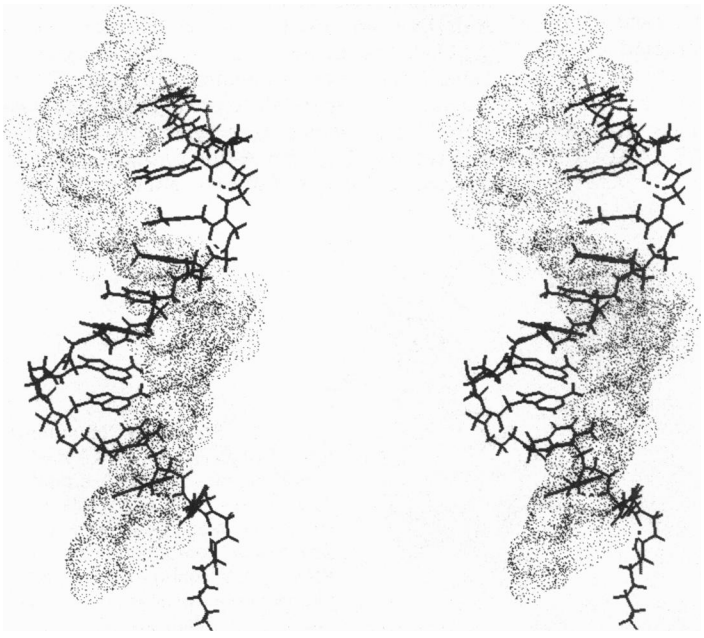

FIG. 3. Stereoview of structure of DNA·PNA hybrid duplex d(CGCAAATTTGCG)/($_{pna}$GCGTTTAAACGC), derived from the solution NMR structure of the d(CGCAAATTTGCG)$_2$ B-DNA dodecamer. PNA strand is represented as stick-structure. Interresidue hydrogen bonds (*a* in Scheme II) stabilize the helical conformation of the PNA strand.

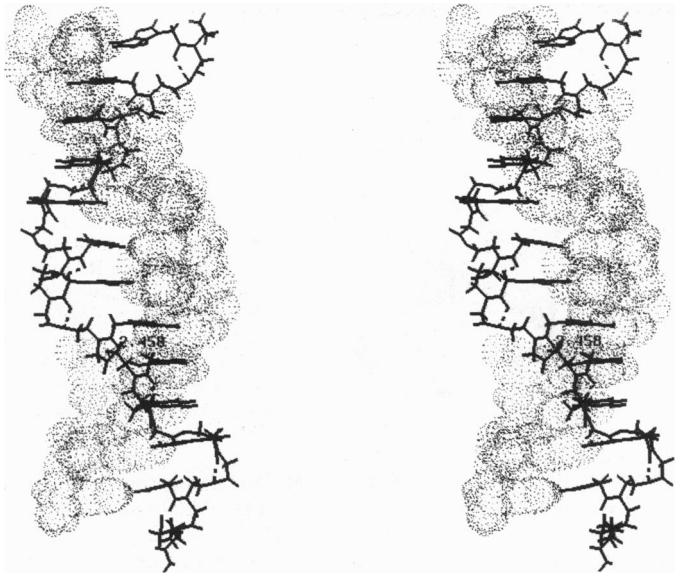

FIG. 4. Stereoview of structure of {d[($_{anti}$Cp)($_{syn}$Gp)]$_6$}·[$_{pna}$(GC)$_6$] DNA·PNA hybrid duplex. The DNA strand, shown as a van der Waals dot surface, is in the Z-conformation. The bases on both strands possess alternating syn and anti conformation with respect to the glycosidic bond, while the PNA strand displays contiguous interresidue hydrogen bonds (see *a* in Scheme II).

helical structures of B-[(dAp)$_{10}$·($_{pna}$T)$_{10}$], A-[(dAp)$_{10}$·($_{pna}$T)$_{10}$], Z-[(dAp)$_{10}$·($_{pna}$T)$_{10}$], and A-[(Ap)$_{10}$·($_{pna}$T)$_{10}$] was assessed by building the PNA strand to favor either interresidue or intraresidue hydrogen bonding. A portion of B-[(dAp)$_{10}$·($_{pna}$T)$_{10}$] with intraresidue hydrogen bonds is shown in Fig. 5. The bottom half of Table 1 lists the various potential energies for the ($_{pna}$T)$_{10}$ strands of B-, A-, and Z-[(dAp)$_{10}$·($_{pna}$T)$_{10}$] as well as A-[(Ap)$_{10}$·($_{pna}$T)$_{10}$], stabilized by intraresidue hydrogen bonding in the PNA strands. For A- and Z-[(dAp)$_{10}$·($_{pna}$T)$_{10}$], the angle deformation and van der Waals energies are lower for intraresidue-hydrogen-bonded T$_{10}$ than for interresidue-hydrogen-bonded structures, although the hydrogen bonding and electronic (coulombic) energies are lowest for interresidue hydrogen bonding. The total potential energies from molecular mechanics calculations are lowest for interresidue-hydrogen-bonded PNA strands in B-[(dAp)$_{10}$·($_{pna}$T)$_{10}$]. Previously, we determined that the PNA strand of B-[(dAp)$_{10}$·($_{pna}$T)$_{10}$] with interresidue hydrogen bonds exists at a local minimum because energy minimization of the helical PNA strand in the absence of the complementary DNA strand resulted in a structure with retained nucleobase orientation and symmetry (5). This is not true when the ($_{pna}$T)$_{10}$ is constructed so that there is intraresidue hydrogen bonding in B-[(dAp)$_{10}$·($_{pna}$T)$_{10}$]. In this structure, energy minimization leads to some disruption of the base orientations. The hydrogen-bond lengths in intraresidue-hydrogen-bonded ($_{pna}$T)$_{10}$ strands are consistently longer than in interresidue-stabilized strands, and this is reflected in increases in the hydrogen bond energies (Table 1). Thus, interresidue hydrogen bonds are stronger than intraresidue hydrogen bonds and are proposed to be favored by this measure.

PNA strands are able to achieve stability in a complementary helical conformation via formation of seven-membered hydrogen-bonded rings (Scheme II) in all characteristic polymorphic states of helical nucleic acids. Comparisons of interresidue-hydrogen-bonded rings in the PNA strands of A-, B-, and Z-{[dAp]$_{10}$·($_{pna}$T)$_{10}$} and A-{[Ap]$_{10}$·($_{pna}$T)$_{10}$} are shown in Fig. 6. The interresidue-hydrogen-bonded ring structure is quite similar in all polymorphs, whereas the conformation of the ethylamine portion of the backbone differs. Comparison of the ($_{pna}$T)$_{10}$ strand conformations in A- and B-[(dA)$_{10}$·($_{pna}$T)$_{10}$] reveals average dihedral angles for rotation around the ethylamine CH_2—CH_2 bond of 90 and 65°, respectively. Thus, complementarity to an A-DNA single strand (and A-RNA single strand) requires eclipsing of a hydrogen on one carbon with the nitrogen substituent on the other methylene, while with a single-strand B-DNA the conformation around the C—C bond is gauche-cis (Fig. 6).

DNA·PNA and RNA·PNA duplexes must be formed as intermediates *en route* to DNA·PNA$_2$ and RNA·PNA$_2$ triplex hybrids. The second PNA likely binds in the major groove of the DNA·PNA intermediate by Hoogsteen base-pairing (Scheme III) (3–5). It is of considerable interest to understand the relative orientations of the two PNA strands in the

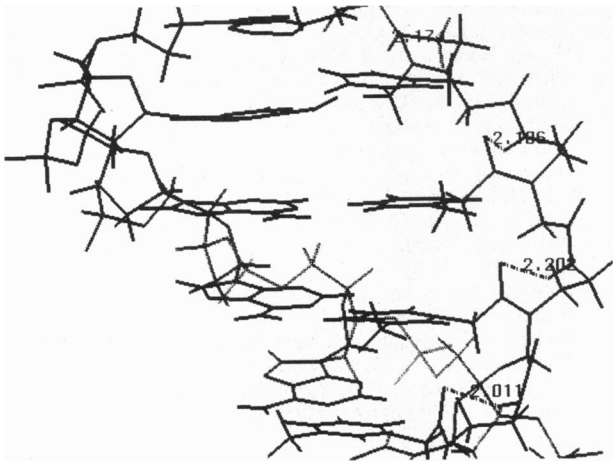

FIG. 5. Close-up view of B-[(dAp)$_{10}$·($_{pna}$T)$_{10}$] with intraresidue hydrogen bonds (see *b* in Scheme II), stabilizing the helical conformation of the PNA strand. Hydrogen bonds are shown as dashed lines and range from 2.0 to 2.2 Å.

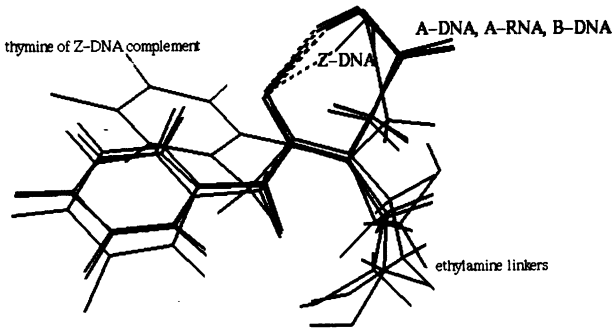

FIG. 6. Overlap of PNA structures when complementary to Z-DNA, B-DNA, A-RNA, and A-DNA. Least-squares fitting was performed for the rings in each decamer of complementary PNA.

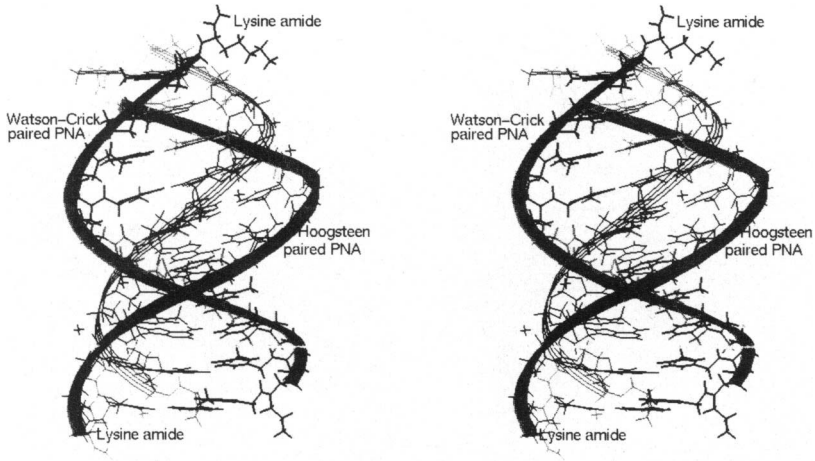

FIG. 7. Stereoview of structure of $(dAp)_{10}\cdot[(_{pna}T)_{10}]_2$ DNA–PNA_2 hybrid triplex, with the DNA strand in the B-conformation. Interresidue hydrogen bonds (see *b* in Scheme II) stabilize the helical conformations of the PNA strands that are antiparallel to one another. The solid ribbon traces lie through the backbone of the PNA strands, whereas the $(dAp)_{10}$ strand backbone is traced with a ribbon of lines.

$DNA\cdot PNA_2$ and $RNA\cdot PNA_2$ products. In an attempt to address this aspect, structures for B-$\{(dAp)_{10}\cdot[pnaT_{10}]_2\}$ and

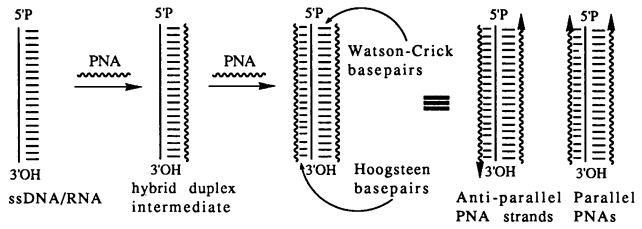

Scheme III

A-$\{(Ap)_{10}\cdot[pnaT_{10}]_2\}$ triple helices were modeled, where the PNA strands are in parallel and antiparallel orientations to one another (Scheme III). A structure for the antiparallel arrangement of two $(_{pna}T)_{10}$ strands in a triplex with B-DNA $(dAp)_{10}$ is shown in stereoview in Fig. 7. The potential energies for each PNA strand conformation in B-$\{(dAp)_{10}\cdot[(_{pna}T)_{10}]_2\}$ and A-$\{(Ap)_{10}\cdot[(_{pna}T)_{10}]_2\}$ were calculated in the absence of complementary DNA by molecular mechanics. The structures of A-$\{(Ap)_{10}\cdot[(_{pna}T)_{10}]_2\}$ with $(_{pna}T)_{10}$ strands parallel and antiparallel are very similar in potential energy. Van der Waals energy for the parallel structure is somewhat lower in the Hoogsteen strand (−78.7 kcal/mol) than in the Watson–Crick PNA strand (−68.3 kcal/mol). Angle-deformation energies are higher in the Hoogsteen strands (−130 kcal/mol) than in Watson–Crick strands (−118 kcal/mol). For B-$\{(dAp)_{10}\cdot[(_{pna}T)_{10}]_2\}$, Watson–Crick pairing of $(_{pna}T)_{10}$ is favored energetically over Hoogsteen base pairing, largely due to unfavorable angle and dihedral contributions. Thus, the angle terms for the Watson–Crick and Hoogsteen PNA strands of antiparallel B-$\{(dAp)_{10}\cdot[(_{pna}T)_{10}]_2\}$ are 104.4 and 114.1 kcal/mol, respectively. The dihedral contributions are found to be 48.8 and 92.7 kcal/mol, respectively. In addition, van der Waals and hydrogen-bonding energies are less negative for the Hoogsteen-paired strands than observed in the Watson–Crick $(_{pna}T)_{10}$ strands. B-$\{(dAp)_{10}\cdot[(_{pna}T)_{10}]_2\}$ with $(_{pna}T)_{10}$ strands antiparallel have lower potential than the parallel structure.

The extraordinary capability of PNA to perform strand invasion into B-$(dAp)_n\cdot(dTp)_n$ sequences by displacing a portion of the complementary DNA and ultimately giving $DNA\cdot PNA_2$ (14) can be rationalized in terms of the considerably lower potential energies for the Watson–Crick compared with the Hoogsteen strands. The initial binding of PNA to dsDNA may be through Hoogsteen base-pairing in the major groove, followed by rearrangement into the more stable Watson–Crick base-paired DNA·PNA plus single-stranded DNA.

Comment. We add that we do not believe that DNA or RNA duplexes with PNA necessarily assume classical A-, B-, or Z-helical structures. Just as the helical structure of a DNA–RNA duplex is partway between an A- and a B-helix (15), duplexes of DNA or RNA with PNA are expected to possess their own characteristics. What we have shown is that (*i*) PNA helical structures are stabilized by interresidue hydrogen bonding, and (*ii*) some flexibility in the seven-membered hydrogen-bonded ring and a good deal of flexibility in the ethylamine component allow the PNA to be complementary to any number of helical arrangements.

We express gratitude to the Office of Naval Research and to the National Science Foundation for support of this work and the computational facilities of this laboratory.

1. Uhlmann, E. & Peyman, A. (1990) *Chem. Rev.* **90,** 543–580.
2. Garner, P. & Yoo, J. U. (1993) *Tetrahedron Lett.* **34,** 1275–1278.
3. Nielsen, P. E., Egholm, M., Berg, R. H. & Buchardt, O. (1991) *Science* **254,** 1497–1500.
4. Egholm, M., Buchardt, O., Nielsen, P. E. & Berg, R. H. (1992) *J. Am. Chem. Soc.* **114,** 1897–1898.
5. Almarsson, Ö., Bruice, T. C., Kerr, J. M. & Zuckermann, R. N. (1993) *Proc. Natl. Acad. Sci. USA* **90,** 7518–7522.
6. Blaskó, A., Browne, K. A., He, G.-X. & Bruice, T. C. (1993) *J. Am. Chem. Soc.* **115,** 7080–7092.
7. Brooks, B. R., Bruccoleri, R. E., Olafson, B. D., States, D. J., Swaminathan, S. & Karplus, M. (1983) *J. Comput. Chem.* **4,** 187–217.
8. Saenger, W. (1984) *Principles of Nucleic Acid Structure* (Springer, New York), pp. 122–126.
9. Wang, A. H.-J., Quigley, G. J., Kolpak, F. J., van der Marel, G., van Boom, J. H. & Rich, A. (1981) *Science* **211,** 171–176.
10. Nielsen, P. E., Egholm, M., Berg, R. H. & Buchardt, O. (1993) *Clin. Chem.* **39,** 715 (abstr.).
11. Nielsen, P. E., Egholm, M., Berg, R. H. & Buchardt, O. (1993) *Anti-Cancer Drug Des.* **8,** 53–63.
12. Hanvey, J. C., Peffer, N. J., Bisi, J. E., Thomson, S. A., Cadilla, R., Josey, J. A., Ricca, D. J., Hassman, C. F., Bonham, M. A., Au, K. G., Carter, S. G., Bruckenstein, D. A., Boyd, A. L., Noble, S. A. & Babiss, L. E. (1992) *Science* **258,** 1481–1485.
13. Rich, A., Nordheim, A. & Wang, A. H.-J. (1984) *Annu. Rev. Biochem.* **53,** 791–846.
14. Nielsen, P. E., Egholm, M., Berg, R. H. & Buchardt, O. (1993) *Nucleic Acids Res.* **21,** 197–200.
15. Salazar, M., Fedoroff, O. Y., Miller, J. M., Ribeiro, N. S. & Reid, B. R. (1993) *Biochemistry* **32,** 4207–4215.